

Article

Investigation on the Impact of Different Absorber Materials in Solar Still Using CFD Simulation—Economic and Environmental Analysis

Chandrakant Sonawane ¹, Ali Jawad Alrubaie ², Hitesh Panchal ³, Ali J. Chamkha ⁴, Mustafa Musa Jaber ^{5,6}, Ankit D. Oza ⁷, Sasan Zahmatkesh ⁸, Dumitru Doru Burduhos-Nergis ^{9,*} and Diana Petronela Burduhos-Nergis ^{9,*}

- ¹ Department of Mechanical Engineering, Symbiosis Institute of Technology, Symbiosis International (Deemed University), Pune 412115, Maharashtra, India
- ² Department of Medical Instrumentation Techniques Engineering, Al-Mustaqbal University College, Hilla 51001, Iraq
- ³ Department of Mechanical Engineering, Government Engineering College, Patan 384265, Gujarat, India
- ⁴ Faculty of Engineering, Kuwait College of Science and Technology, Doha 35004, Kuwait
- ⁵ Department of Medical Instruments Engineering Techniques, Dijlah University College, Baghdad 10021, Iraq
- ⁶ Department of Medical Instruments Engineering Techniques, Al-Turath University College, Baghdad 10021, Iraq
- ⁷ Department of Computer Sciences and Engineering, Institute of Advanced Research, The University for Innovation, Gandhinagar 382426, Gujarat, India
- ⁸ Department of Chemical Engineering, University of Science and Technology of Mazandaran, Behshahr P.O. Box 48518-78195, Iran
- ⁹ Faculty of Materials Science and Engineering, Gheorghe Asachi Technical University of Iasi, 700050 Iasi, Romania
- * Correspondence: doru.burduhos@tuiasi.ro (D.D.B.-N.); diana.burduhos@tuiasi.ro (D.P.B.-N.)



Citation: Sonawane, C.; Alrubaie, A.J.; Panchal, H.; Chamkha, A.J.; Jaber, M.M.; Oza, A.D.; Zahmatkesh, S.; Burduhos-Nergis, D.D.; Burduhos-Nergis, D.P. Investigation on the Impact of Different Absorber Materials in Solar Still Using CFD Simulation—Economic and Environmental Analysis. *Water* **2022**, *14*, 3031. <https://doi.org/10.3390/w14193031>

Academic Editor: Yakun Guo

Received: 19 August 2022

Accepted: 21 September 2022

Published: 27 September 2022

Publisher's Note: MDPI stays neutral with regard to jurisdictional claims in published maps and institutional affiliations.



Copyright: © 2022 by the authors. Licensee MDPI, Basel, Switzerland. This article is an open access article distributed under the terms and conditions of the Creative Commons Attribution (CC BY) license (<https://creativecommons.org/licenses/by/4.0/>).

Abstract: Solar stills are one of the low water production desalination systems, but its low yield makes it necessary to investigate different design and performance parameters to improve its productivity. This paper aims to perform a parametric analysis of a solar still desalination system and study the effect of different absorber materials on the performance of a single-slope solar desalination unit employing computational fluid dynamics (CFD) numerical simulation via COMSOL[®] Multiphysics software. To consider the absorptivity of water with different absorbing materials, simulation was conducted with the application of effective emissivity for the solar still walls. In addition, the economic, exergoeconomic, and CO₂ mitigation of solar stills were studied. The results revealed that the hourly water output of the solar desalination unit, with different absorbing materials (black ink, black dye, and black toner), reached the maximum values at 1:00 PM. On comparing the simulation results of solar stills with and without absorbing materials, it has been observed that the solar still painted with black toner shows the highest improvement in hourly productivity, the exergy of evaporation, and evaporative heat transfer coefficient with a maximum increase in respective values by 10.52%, 13.68% and 5.37%. The CO₂ mitigation and enviroeconomic parameter of the solar still using black toner were equal to 31.4 tons and 455.3 USD, respectively. Moreover, the lowest cost per liter (CPL) of the solar still was obtained using black toner, which was about 0.0066 USD/L.

Keywords: solar desalination; absorber; effective emissivity; exergy; CFD simulation

1. Introduction

Water is an inevitable component of the existence of living beings, while potable water is necessary for the sustainable development of human beings [1]. Although about three quarters of the earth's surface is occupied with water, available freshwater for human consumption is limited to only about 1% [2]. Global freshwater demand for domestic,

industrial, and agricultural usage will significantly increase [3]. Desalination is the method used to obtain freshwater from saline water. The most popularly used desalination technologies across the globe are multi-effect distillation (MED), multistage flashing (MSF), and reverse osmosis (RO) [4], but these systems require electric energy. These systems are expensive for common people and not feasible for people living in remote areas. Solar desalination can be a sustainable choice to obtain freshwater from saline water. A solar still is one of the low-cost devices used for the solar desalination process in most of the Arabic regions due to ample solar radiation availability throughout the year.

The freshwater output of solar-based desalination using solar stills is usually low; thus, it is essential to investigate various parameters that can help in the design of the solar still to increase freshwater generation. In order to increase water temperature and accelerate evaporation rate in the solar still, which consequently improves freshwater production, many researchers have integrated different components in solar desalination systems such as flat plate collector [5], mirrors [6], solar concentrator [7], evacuated tubes collector [8], photovoltaic/thermal [9], external condenser [10], and glass cover cooling [11]. Using an external condenser also improves the clean water generation of solar desalination.

Researchers have investigated the thermal performance of solar stills under different metrological and operating conditions [12]. Water depth in the basin, as well as the absorber plate geometry of the solar still significantly affects distillate output [13,14]. Researchers have also investigated the impact of energy storage media on the performance of solar desalination by the application of different materials such as phase change material (PCM) [15], nano-enhanced PCM [16], jute [17], black granite gravels [18], exfoliated graphite coating [19], black toner [20], black ink and black dye [20], etc. Energy analysis of a thermal system provides the quantity-wise evaluation of energy, while exergy analysis provides a quality-wise evaluation of energy [21]. Exergy analysis helps to understand the heat transfer process and can be applied to reduce exergy destruction, thus improving the output of a thermal desalination unit. Deniz [22] designed a desalination system integrated into a flat plate collector and analyzed it with the help of energy and exergy efficiencies. They indicated that ambient conditions, including solar irradiation, ambient temperature, and wind velocity, affected energy and exergy efficiencies. Sharshir et al. [12] reviewed different solar still designs and studied operating parameters with the help of energy and exergy analysis. They revealed that there are unexplored research areas due to complexity in analysis or experiment performance.

A numerical simulation is an analysis tool that has the ability to deal with various types of complex systems [23–25]. Computational fluid dynamics (CFD) analysis may play a crucial role in optimizing water production, energy consumption, and cost of thermal-based desalination units. The design of solar desalination by numerical study allows us to define all the essential parameters of solar desalination within an acceptable error and achieve the highest water production rate by changing critical parameters, including energy storage media and absorber surface. Akbar and Ismail [26] investigated the multistage solar still using evacuated tubes by means of numerical simulations. They used a finite element analysis (FEA) model to simulate the evaporation and condensation process in solar desalination. Badusha and Arjunan [27] developed a volume of fraction (VOF) model in ANSYS Fluent to simulate temperature, mass flow, and volume fraction of water vapor in single-slope solar desalination. Rahbar and Eshafani [28] used a two-dimensional CFD analysis to predict the hourly performance of a solar still. They proposed a model of the Chilton–Colburn analogy to estimate the water output of the solar still.

Rahbar et al. [29] carried out a numerical study of tubular solar desalination to predict the water generation of the system. They established correlation formulas to compute water productivity, heat, and mass transfer coefficient as functions of component temperature. Maheswari et al. [30] compared the experimental results of single-basin double-slope solar desalination with the corresponding simulation results obtained by ANSYS CFX 14.0 software. They revealed that a good agreement had been obtained between experimental results and numerical data. Furthermore, the effects of solar irradiance received for differ-

ent months, ambient temperature, and wind velocity on the generation of solar still were observed. Hafs et al. [31] studied a solar still considering the application of nanofluid and phase change material using COMSOL[®] software. They observed that the daily productivity of solar desalination with and without phase change material increased by 48% and 27% compared to a conventional still. Sharshir et al. [32] experimentally investigated the effect of different basin metals and wick-metal chips pad on the performance of an inclined wick solar still. They studied temperature distribution in this system with the help of COMSOL[®] Multiphysics software. The outcomes revealed a good agreement between experimental and simulation results.

Shoeibi et al. [33] evaluated the effect of water and glass cooling on the performance of water-cooled and air-cooled solar stills using CFD simulation. The different operating parameters of a solar still, including water cooling temperature, glass cover thickness, and velocity of water glass cooling, were studied. Their results indicated that the water productivity of a solar still using water glass cooling improved by about 21.53% compared with an air glass cooling solar still. In another study by Shoeibi et al. [34], the effect of hybrid nanofluid glass cooling using CFD simulation was evaluated. Al₂O₃-TiO₂/water hybrid nanofluids were used to decrease the glass cover temperature of the solar desalination. Their results revealed that the optimum volume fraction of the hybrid nanofluid was about 0.45%.

Further, a simulation study of different types of solar distiller has been reviewed [35], which included: single-slope solar distiller, double-slope solar distiller, tubular solar still distiller, inclined solar distiller, double-basin solar distiller, humidification and dehumidification system, vapor compression desalination system, and desalination system integrated with parabolic trough collector, ensuring CFD as a valuable tool for validation of various solar desalination. Recently, Fan et al. [36,37] demonstrated the CFD simulation for panel surface cleaning applications. Sonawane et al. [38–40] have also summarized the detailed bibliometric-based review on CFD-modelled simulation for solar desalination application. A few other relevant works related to CFD modelling and solar desalination include [41–47].

It is observed that the different configurations of solar desalination systems have been investigated using experimentation, energy analysis, exergy analysis, and numerical simulation. Many studies have used CFD simulation to analyze solar stills considering the application of nanofluid, phase change material, and porous absorber. There are also many parameters of the solar desalination system that can be explored through CFD analysis. To the best of the authors' knowledge, the investigation of various absorber materials used in solar stills to improve freshwater production using CFD simulation has not been evaluated yet. The aim of this paper is to conduct a parametric analysis of a solar still and investigate its performance for different absorber materials used in solar still desalination by CFD simulation. The present paper uses the results of Layek [20] to compare the experimental results with numerical simulation of the model using COMSOL[®] Multiphysics software version 5.6, Comsol Inc (Stockholm, Sweden). [48]. Furthermore, the economic, exergoeconomic, and CO₂ mitigation analysis of the system was studied.

2. Model Description

2.1. Physical Model

A single-slope solar desalination system, as shown in Figure 1, is one of the popularly explored systems with readily available experimental results. Hence, we have selected a single-slope solar desalination with the absorber plate area of 1.3 m × 0.8 m, as mentioned in the experimental work [20]. The cover with 0.3 cm thickness and inclination of 23° was considered to better direct the distilled water to the outlet. A thin galvanized iron sheet was used to fabricate the solar still, and the enclosure body was insulated by glass wool with a thickness of 0.05 m. The inner surface of the still basin was covered with black paint to raise its absorptivity. The absorber materials, including the black ink solution and the

black dye solution mixed in the water and the black toner, were placed on the water surface to increase the solar absorptivity of water. Specifications of the model are given in Table 1.

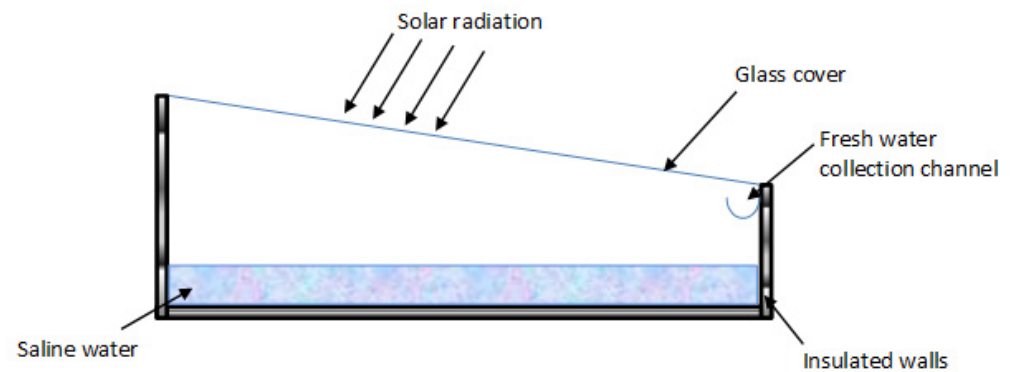


Figure 1. Schematic diagram of a single-slope solar still.

Table 1. The model specifications.

Parameter	Values
Absorptivity of basin liner, (α_b)	0.90
Absorptivity of water, (α_w)	0.30
Absorptivity of water with black ink, (α_w)	0.43
Absorptivity of water with black dye, (α_w)	0.57
Absorptivity of water with black toner, (α_w)	0.70
Transmissivity of water, (τ_w)	0.67
Transmissivity of water with black ink, (τ_w)	0.54
Transmissivity of water with black dye, (τ_w)	0.41
Transmissivity of water with black toner, (τ_w)	0.28

2.2. Mathematical Model

In order to apply radiation to the solar still model for CFD analysis in COMSOL[®] Multiphysics 5.6 software, the “heat transfer with surface-to-surface radiation” module has been used. The step by step description of COMSOL modelling is prescribed in Appendix A. Total radiative (thermal) flux leaving a surface can be evaluated as follows [49]:

$$Q_{ij} = A_i F_{ij} (J_i - J_j) \quad (1)$$

where Q_{ij} , A_i , F_{ij} , J_i and J_j show the thermal power transmitted from body “i” to body “j”, the surface area of body “i”, the view factor from body “i” to body “j”, total radiative flux leaving surface “i” and total radiative flux leaving surface “j”, respectively. All surfaces and objects are considered to possess isothermal properties. Thermal black body radiation transmitted from a surface is obtained as follows:

$$Q_i = \frac{A_i \varepsilon_i (\sigma T_i^4 - J_i)}{1 - \varepsilon_i} \quad (2)$$

where Q_i , ε_i , σ and T_i present the thermal energy leaving surface “i”, the thermal (infrared) emissivity of surface “i”, Stefan Boltzmann coefficient and the temperature of surface “i”, respectively. The radiation flux, in equilibrium, between two surfaces of different temperatures is then given by:

$$Q_{ij} = \sigma A_i \varepsilon_i (T_i^4 - T_j^4) \quad (3)$$

In addition, the view factor can be defined as radiation from surface “*i*” intercepted by surface “*j*”.

$$F_{ij} = \frac{\text{radiation emitted from } A_i \text{ and incident on } A_j}{\text{total radiation emitted from } A_i} \quad (4)$$

The following equations were described to understand the “heat and moisture transport” module used in the COMSOL[®] Multiphysics software. The heat transfer through the fluids’ interface was explained using the following equation:

$$\rho C_p \left(\frac{\partial T}{\partial t} + u \cdot \nabla T \right) + \nabla \cdot (q + q_r) = \alpha_p T \left(\frac{\partial p}{\partial t} + u \cdot \nabla p \right) + \tau : \nabla u + Q \quad (5)$$

where *Q* and *q* indicate the heat sources other than viscous dissipation and heat flux by conduction, respectively.

The heat transfer through moist air was explained using the following equation:

$$\rho C_p \left(\frac{\partial T}{\partial t} + u \cdot \nabla T \right) + \nabla \cdot (q + q_r) = \left(\frac{\partial p}{\partial t} + u \cdot \nabla p \right) + \tau : \nabla u + Q_H + Q \quad (6)$$

where *Q_H* is the diffusive flux of thermal enthalpy due to the rate of change of air and vapor in moist air and is calculated as follows:

$$Q_H = - (C_{p,v} - C_{p,a}) g_w \cdot \nabla T \quad (7)$$

where *C_{p,v}*, *C_{p,a}* and *g_w* indicate the specific heat capacity at a constant pressure of vapor, the specific heat capacity at a constant pressure of air and vapor flux by diffusion, respectively. When vapor concentration is low, the moisture content variation in terms of the transport of vapor concentration (*c_v*) is expressed as follows:

$$M_v \frac{\partial c_v}{\partial t} + M_v u \cdot \nabla c_v + \nabla \cdot g_w = G \quad (8)$$

$$g_w = -M_v D \cdot \nabla c_v \quad (9)$$

$$c_v = \phi_w c_{sat} \quad (10)$$

where *M_v* and *φ_w* show the molar mass of water vapor and relative humidity, respectively. For larger vapor concentration conditions, the moisture content variation is expressed through the transport of vapor mass fraction *w_v* as follows:

$$\rho_g \frac{\partial w_v}{\partial t} + \rho_g u \cdot \nabla w_v + \nabla \cdot g_w = G \quad (11)$$

$$g_w = -\rho_g D \cdot \nabla w_v \quad (12)$$

$$w_v = \frac{M_v c_v}{\rho_g} \quad (13)$$

where *ρ_g* is the density of moist air. Various absorber materials have been used in the solar still to increase the absorptivity of water. In order to consider the solar absorptivity of water with different absorber materials, the term ‘effective emissivity’ of basin surface has been used. The effective emissivity of basin liner over the solar spectrum is calculated as follows:

$$\varepsilon_{eff} = \alpha_w + \tau_w \times \alpha_b \quad (14)$$

Various methods have been proposed for the evaporation heat transfer coefficient, the most famous of which is the Dunkle correlation [33]:

$$h_{ew} = 0.016273 \times h_{cw} \times \frac{(P_w - P_{gi})}{(T_w - T_{gi})} \quad (15)$$

where h_{cw} shows the convection heat transfer between water and glass and is obtained as follows:

$$h_{cw} = 0.884 \times \left[(T_w - T_{gi}) + \frac{(P_w - P_{gi}) \cdot T_w}{268,900 - P_w} \right]^{\frac{1}{3}} \quad (16)$$

$$P = \text{Exp} \left(25.317 - \frac{5144}{T} \right) \quad (17)$$

Moreover, the evaporation heat transfer can be calculated as follows [50]:

$$q_{ew} = A_b \times h_{ew} \times (T_w - T_{gi}) \quad (18)$$

The hourly yield of distilled water in the solar still is given by:

$$\dot{m}_{ew} = \frac{q_{ew}}{L} \times 3600 \quad (19)$$

where L is the latent heat of vaporization of water (J/kg) and is calculated by the following formula [50]:

$$L = 2.506 \times 10^6 - 2.369 \times 10^3 T + 0.2678 T^2 - 8.103 \times 10^{-3} T^3 - 2.079 \times 10^{-5} T^4 \quad (20)$$

2.3. Exergy Analysis

The exergy generation of the solar still is calculated as follows [50]:

$$Ex_{gen} = \frac{\dot{m}_{ew}}{3600} \times L \times \left(1 - \frac{T_a}{T_w} \right) \quad (21)$$

where Ex_{gen} shows the exergy generation in the system. The exergy of evaporation transferred from water to glass cover is obtained by:

$$Ex_{ew} = A_b \times h_{ew} \times (T_w - T_{gi}) \times \left(1 - \frac{T_a}{T_w} \right) \quad (22)$$

2.4. The Cost of One Litre of Distilled Water

The economic analysis is one of the effective methods to reduce the cost of water generation in solar desalination systems. The capital recovery factor is a technique to estimate effective price and determines the success of an investment and is obtained by [51]:

$$CRF = \frac{i(1+i)^n}{(1+i)^n - 1} \quad (23)$$

where i is the interest rate (8%), and n is the lifespan of the system (20 years). The first annual price of the system is given by [51]:

$$FAC = P \times CRF \quad (24)$$

where P is the capital price of the device. The first annual salvage value is related to the value of devices materials and parts after its lifetime and is shown by [51]:

$$ASV = S \times SSF \quad (25)$$

where S shows the recyclable amount of the device (20% of the material price). The sinking fund factor is considered to estimate the equivalent of the annual price amount at the same price in the specified number of future years and is given by [51]:

$$SSF = \frac{i}{(1+i)^n - 1} \quad (26)$$

The annual maintenance price is dependent on annual costs of goods repair of the system (10% of the first price) and is shown by:

$$AMC = 0.10 \times FAC \quad (27)$$

The uniform annual price of the device is obtained as the following formula [33]:

$$AC = FAC + AMC - ASV \quad (28)$$

Depending on the annual freshwater generation M in the system, the cost per liter of freshwater is obtained as follows [33]:

$$CPL = \frac{UAC}{M} \quad (29)$$

2.5. Exergo-Economic Analysis

The exergoeconomic method is the combination of exergy and economic analysis for determining the cost-effective design of the system and is obtained as follows [33]:

$$R_{Ex} = \frac{(E_{ex})_{out}}{UAC} \quad (30)$$

where E_{ex} and R_{Ex} represent the output exergy and the exergoeconomic parameter, respectively.

2.6. CO₂ Reduction

The CO₂ reduction rate in the system is specified by $(E_{en})_{out} \times 2$. The net amount of CO₂ reduction during the lifetime of the solar still is calculated by [33]:

$$\varphi_{co_2} = \frac{2((E_{en})_{out} \times n - E_{in})}{1000} \quad (31)$$

2.7. Enviroeconomic Analysis

The enviroeconomic term is determined as the price obtained by CO₂ reduction during the system lifetime and is shown by [33]:

$$Z_{co_2} = z_{co_2} \times \varphi_{co_2} \quad (32)$$

where z_{co_2} shows the international carbon cost (14.5 USD per ton of CO₂).

3. Numerical Simulation

3.1. Model Design

A 3D model of the solar still is developed in COMSOL[®] Multiphysics 5.6 software, as shown in Figure 2. The numerical simulation involves multiphysics activities including heat transfer, evaporation, condensation, and phase change effects which can easily be modelled using COMSOL[®] Multiphysics 5.6 software. The dimensions of the solar desalination base area, thickness, inclination of the cover, and thickness of insulation walls are taken as per the experimentation setup [20]. Water depth in the solar still is considered about 2 cm at the start of the test. Boundary conditions, materials, and material properties assigned to the components of the solar still model are listed in Table 2. Due to the very thin galvanized steel sheet used for solar still fabrication is not included in the geometric model. However, emissivity is applied to the model to consider the thermal effect of black paint on the inner wall surfaces of the still and absorber materials added to water.

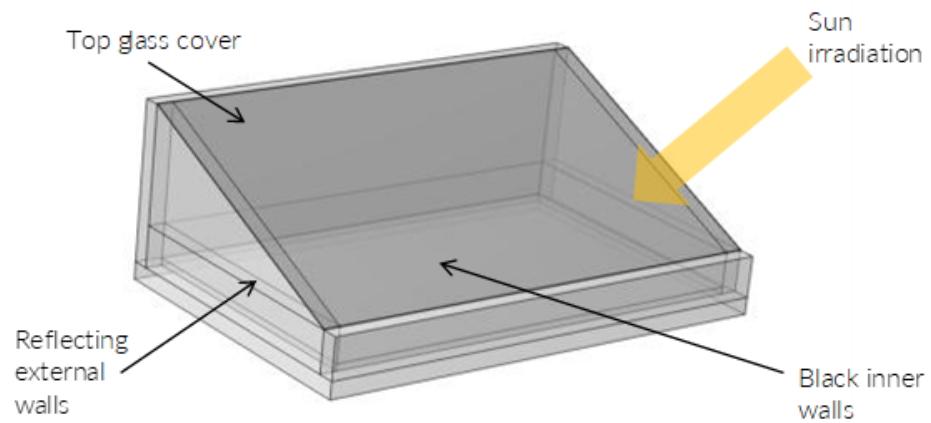


Figure 2. A 3D model of the solar still showing boundary conditions.

Table 2. Boundary conditions and material properties.

Component	Boundary Conditions	Material	Opacity	Thermal Conductivity [W/(m·K)]	Cp [J/(kg·K)]	Surface Emissivity	Heat Transfer Mode
Top cover	Solid	Silica glass	Opaque for infrared radiation	1.38	703	0.03	Conduction; Convective heat flux on outer and inner surfaces
Solar still walls	Solid	Glass wool batt	Opaque	0.034–0.048	850	Outer surface: 0.03	Conduction; Convective heat flux on the surface
						Inner surface (black painted): 0.9	Conduction; Convective heat flux on the surface
Lower domain inside solar still	Fluid	Water, liquid	Transparent	0.56–0.69	4150–4250	-	Convectively enhanced conductivity
Upper domain inside solar still	Fluid	Moist air	Transparent	0.02–0.035	1000–1020	-	Convectively enhanced conductivity

3.2. Simulation Method and Boundary Conditions

The performance of the solar still is simulated with the ‘heat transfer with a surface-to-surface radiation’ module and the ‘heat and moisture transport’ module. The mesh independence of the computational domain was verified using fine and extra fine mesh created in the COMSOL[®] software, as shown in Table 3. Mesh used further for the computational domain is shown in Figure 3, and the domain consists of extra-fine mesh near the solar still walls and water surfaces. Ambient properties are applied to the model as per the location of experimentation. The initial temperature of all the parts of the solar still is considered to be ambient temperature. The convection condition is applied to water and moist air in the enclosure of the solar desalination in order to enhance heat transfer through these fluids. Water is considered a latent heat source for evaporation purposes. Heat flux conditions are applied to all the outer surfaces of the solar still for external natural convection. Note that the assumption of homogenous heating of the liquid phase is utilized here in the simulation work.

Table 3. Mesh models.

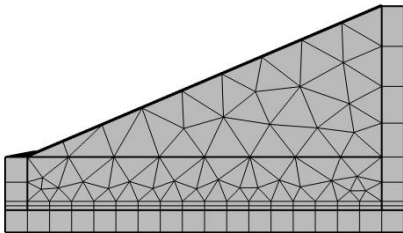
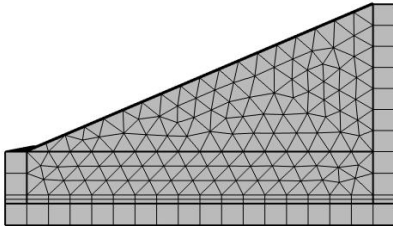
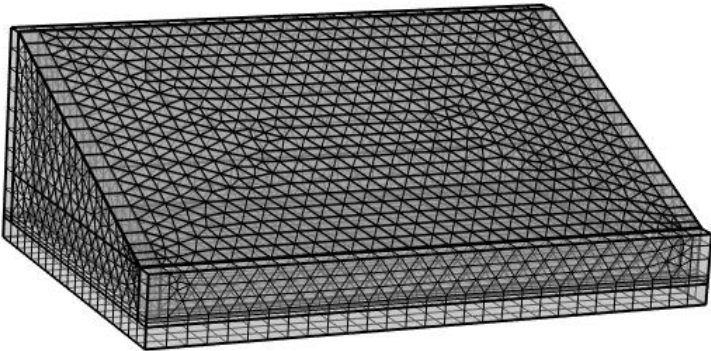

Mesh Model	Description
	<ul style="list-style-type: none"> • Fine mesh near solar still walls and extra fine mesh near water surface. • Number of elements: 7046 Average error: 42.5%
	<ul style="list-style-type: none"> • Extra fine mesh near solar still walls and water surface. • Number of elements: 11,915 Average error: 40.5%
	
	

Figure 3. Mesh model of the solar still.

An external radiation source is applied to the model, with the source position changing as per simulation time according to the position of the sun. Visible light is allowed to pass through the glass cover. Far infrared radiations emitted from inner surfaces of the still are not permeable through the glass, thus increasing the inside temperature. The emissive power of the solar still walls is defined as per the wavelength of radiation. It is operated for higher emissions of the near-visible radiations at higher temperatures.

4. Result and Discussion

4.1. The Components of the Solar Still

The single-slope solar desalination system using various absorber materials was conducted by CFD simulation. Figure 4 shows that the solar irradiations falling on the solar desalination system vary in their direction as per the source position considering the time. As can be seen, the basin liner's temperature increases and transfers the heat to the water by natural convection heat transfer. Figure 5a shows the temperature variation at a middle section plane of the solar desalination. The results showed that the highest temperature of the solar desalination was obtained in the basin liner due to the black cover paint. Figure 5b indicates the H₂O mass fraction contour inside the solar desalination. The evaporation rate of the water surface increases by increasing the different temperatures between glass and water in solar radiation. Temperature variation on the walls of the solar still (as shown

in Figure 6) indicates higher temperature on the outer wall towards the external source. Furthermore, a shadow of the solar still wall causes a lower temperature near that wall inside the solar still.

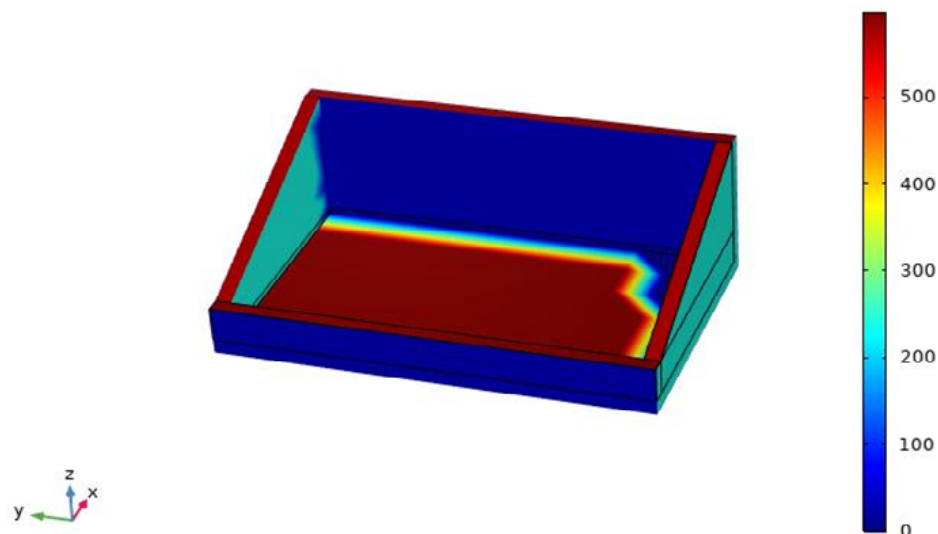
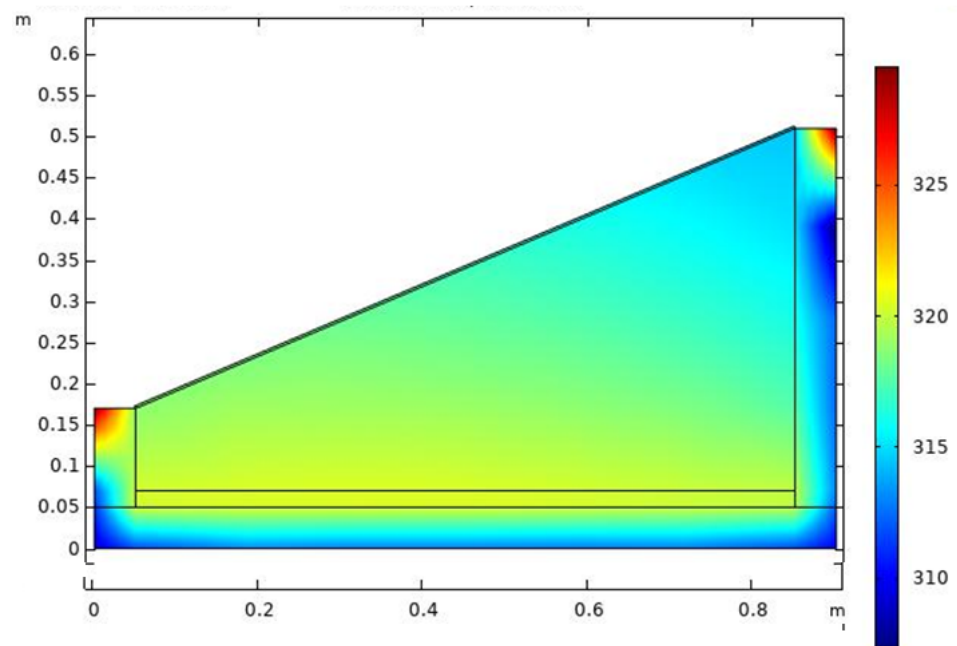


Figure 4. Solar irradiation (in W/m^2) on the solar still (simulation time = 10 am).

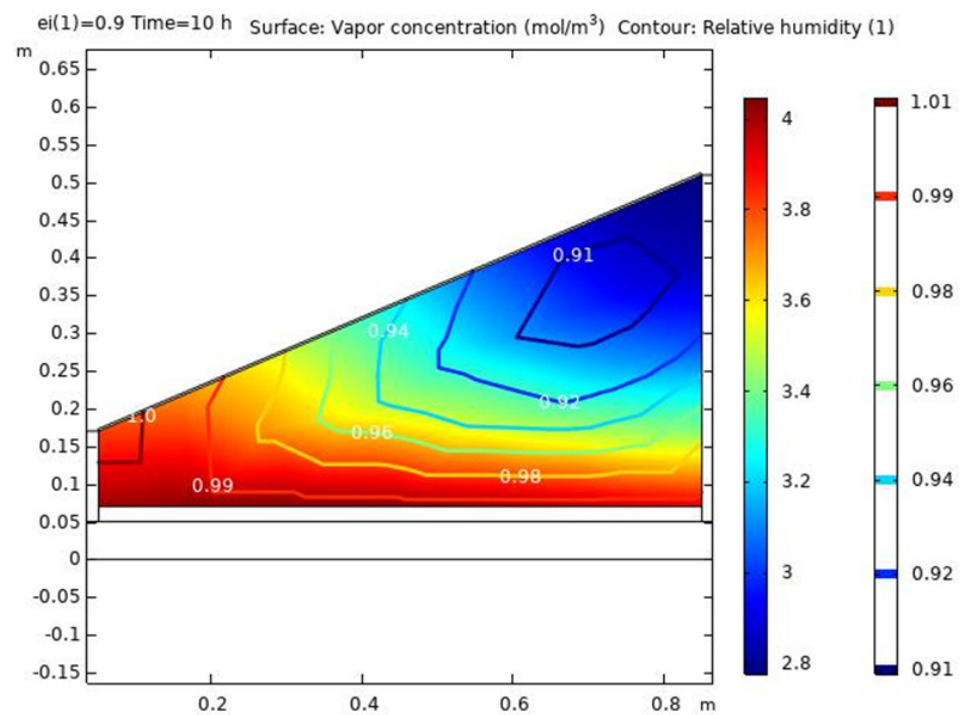
4.2. Parametric Study for Different Absorber Materials

Figure 7 shows experimental [20] and simulation results of water productivity of solar desalination. To simulate the effect of different absorber materials, effective emissivities of the inner wall surfaces of the solar still have been calculated as shown in Equation (14). As shown in Figure 7, the trend of hourly productivity of CFD simulation is similar to that of the experimental data. It can be seen that as the absorptivity of the absorber material increases, the water productivity of the solar still increases. The hourly productivity of the solar desalination rises with time and achieves its highest at 1 PM and then reduces for all the absorber materials due to low solar radiation at the end of the day. As compared to the solar still without the absorber, maximum values of hourly productivity in [20] increase for absorber materials black ink, black dye, and black toner by 15.65%, 21.92%, and 32.88%, respectively, whereas simulated maximum values of hourly productivity increase for the corresponding absorber materials by 4.88%, 8.73%, and 10.52%, respectively.

Figure 8 shows the hourly variations of exergy evaporation during the experiments and CFD simulation results. The results illustrated that the highest exergy evaporation in solar desalination was obtained in the solar still using black toner at 1 PM, which was about 57 W. Moreover, the exergy evaporation of the solar still using black ink was raised by 17.3% compared to solar desalination without absorber material. Figure 9 indicates the hourly trends of evaporative heat transfer coefficient throughout the day for the results in [20] and the simulation results. The results showed that the trend of all configurations of solar stills using different absorber materials is at the same in various hours. As illustrated in Figures 8 and 9, the simulated values are considerably lower than those in [20]. As compared to the solar still with no absorber, maximum values of exergy of evaporation in [20] increase for absorber materials black ink, black dye, and black toner by 16.54%, 24.69%, and 41.48%, respectively, whereas simulated maximum values of exergy of evaporation increase for the corresponding absorber materials by 6.26%, 11.32%, and 13.68%, respectively.



(a)



(b)

Figure 5. (a) Simulation results of temperature variation of the solar still (in K) (simulation time = 10 AM). (b) Simulation results of moisture concentration and relative humidity inside the solar desalination (simulation time = 10 AM).

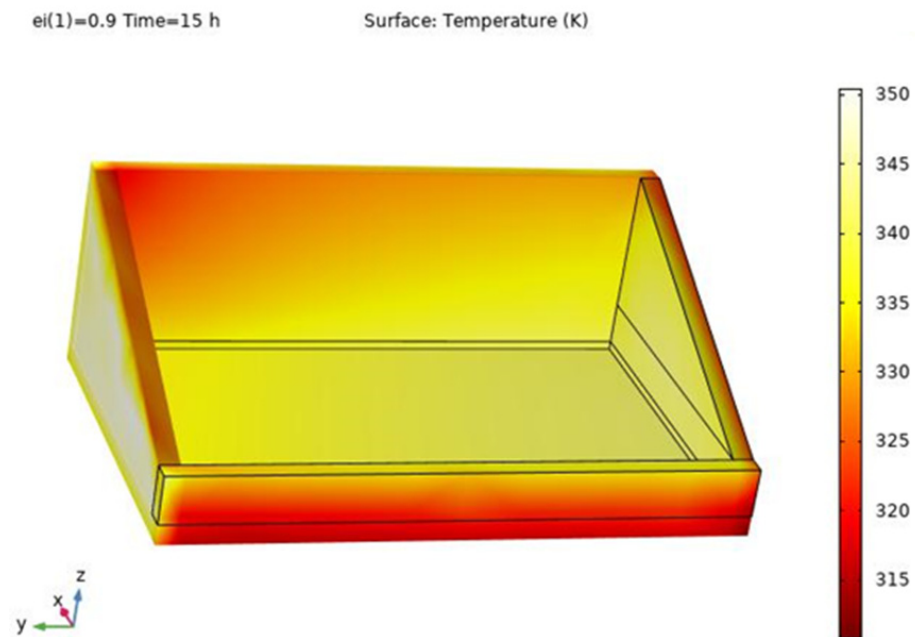


Figure 6. Temperature variation (in K) on walls of the solar still (simulation time = 3 PM).

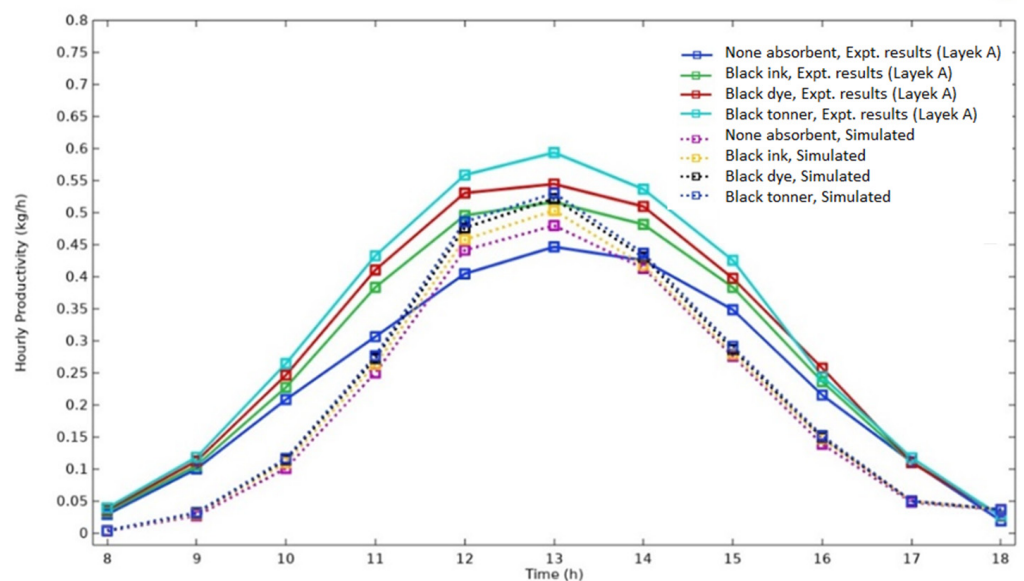


Figure 7. The hourly yield of the solar still.

Similarly, considering the solar still with no absorber, maximum values of evaporative heat transfer coefficient in [20] increase for absorber materials black ink, black dye, and black toner by 16.32%, 20.40%, and 32.65%, respectively, whereas simulated highest values of evaporative heat transfer coefficient increase for the corresponding absorber materials by 2.45%, 4.46%, and 5.37% respectively. From the simulation results, maximum values of exergy of evaporation and heat transfer coefficient are considerably lower than that of the results in [20]. Furthermore, the simulated results show higher values of all results at 6 PM as compared to corresponding values in [20]. The simulated and experimental values are due to the difference between calculated and actual heat transfer rates from water to glass cover and from glass cover to the outside air.

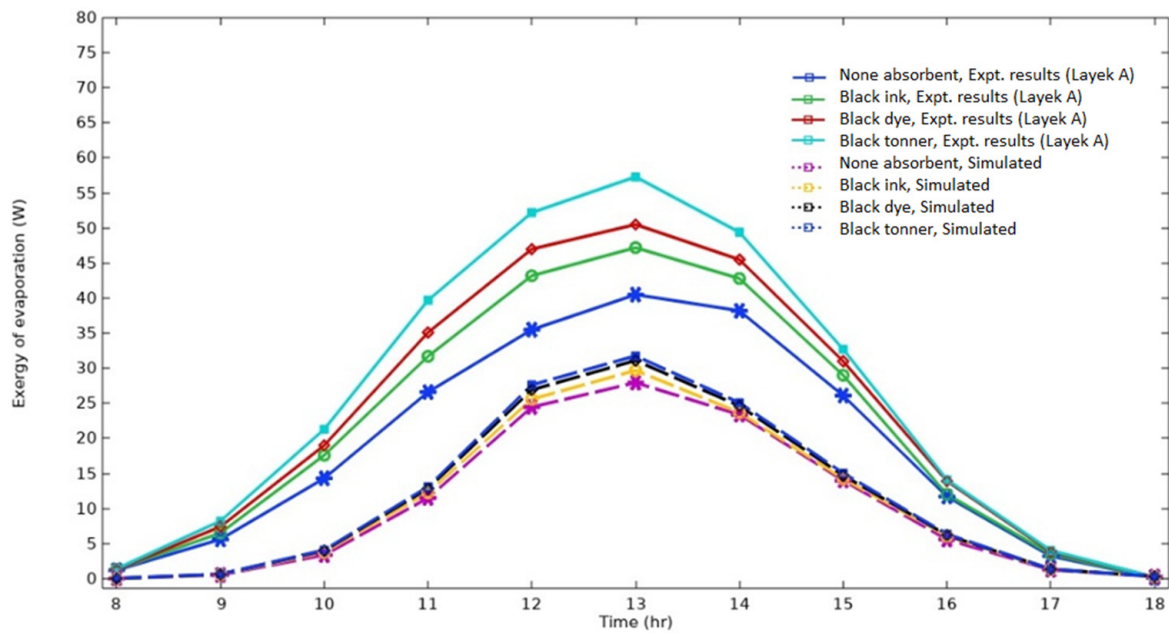


Figure 8. Exergy of evaporation of the solar still for different absorbers in water.

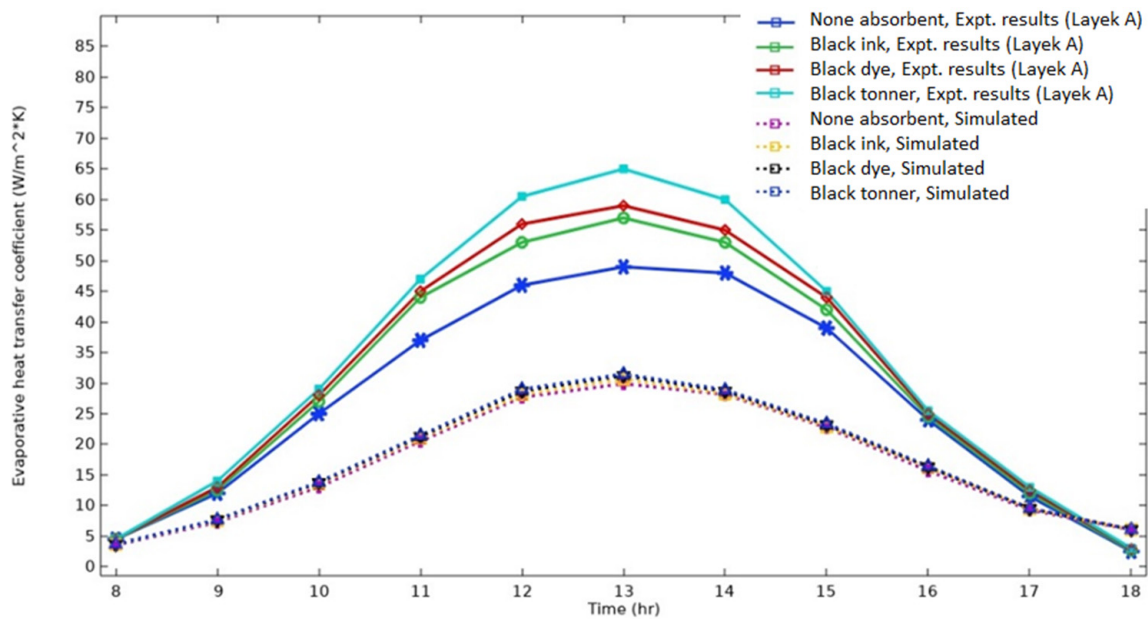


Figure 9. Evaporative heat transfer coefficient (h_{ew}) for various absorbing materials in water.

4.3. Environmental and Exergoeconomic Parameters

Table 4 shows the value of fabrication of the solar desalination. The obtained results showed that the cost of the system and salvage value of the solar still are about 75 USD and 15 USD, respectively. Table 4 indicates the CPL of the system using different absorber materials. Results revealed that the lowest CPL of the solar still was obtained by using black tonner, which was about 0.0066 USD/L. Table 5 summaries the economic analysis for different absorbent materials.

Table 4. Cost of fabricated of single-slope solar still using absorber materials.

Solar Still's Material	Cost of System (USD)	Salvage Value (USD)
Galvanized iron sheet	35	7
Glass cover	5	1
Galvanized support	15	3
Glass wool insulation	10	2
Black ink/toner	10	2
Total cost	75	15

Table 5. Economic analysis of solar desalination using different absorber material.

Type	n (Year)	i (%)	CRF	FAC (USD/Year)	SFF	S (USD)	ASV (USD/Year)	AMC (USD/Year)	UAC (USD/Year)	M (m ³ /Year)	CPL (USD/L)
Conventional solar still	20	0.08	0.102	7.64	0.02	15.0	0.33	0.76	8.08	967	0.0083
Solar still with Black Toner	20	0.08	0.102	7.64	0.02	15.0	0.33	0.76	8.08	1228	0.0066
Solar still with Black Dye	20	0.08	0.102	7.64	0.02	15.0	0.33	0.76	8.08	1165	0.0069
Solar still with Black Ink	20	0.08	0.102	7.64	0.02	15.0	0.33	0.76	8.08	1109	0.0073

Table 6 indicates the energy, exergy production, and exergoeconomic parameters based on energy and exergy of different solar stills. The outcomes show that the highest energy and exergy production occurred in the solar still using black toner, which is about 785 kWh and 49.8 kWh, respectively. In addition, the exergoeconomic based on energy and exergy of solar desalination using black dye is equal to 92.14 kWh/USD and 6.17 kWh/USD, respectively.

Table 6. Exergoeconomic parameter of different solar desalination.

Type	Life Time	i (%)	(kWh) (E _{ex}) _{out}	(kWh) (E _{en}) _{out}	UAC	R _{En} (kWh/USD)	R _{Ex} (kWh/USD)
Conventional solar still	20	0.08	39.24	618	8.08	76.53	4.86
Solar still with Black Toner	20	0.08	49.8	785	8.08	97.19	6.17
Solar still with Black Dye	20	0.08	47.2	745	8.08	92.14	5.85
Solar still with Black Ink	20	0.08	45.0	709	87.86	8.08	5.57

Table 7 illustrates the CO₂ reduction and enviroeconomic parameters in the desalination system. The results revealed that the CO₂ mitigation and enviroeconomic parameter of the solar still using black toner were equal to 31.4 tons and 455.3 USD, respectively, during a life span. Moreover, the CO₂ removal of the solar still by black dye was improved by about 4.9% compared to the solar still using black ink.

Table 7. CO₂ mitigation of different solar stills.

Type	Life Time	CO ₂ Mitigation (Tons)	Enviroeconomic Parameter (USD)
Conventional solar still	20	24.7	358.4
Solar still with Black Toner	20	31.4	455.3
Solar still with Black Dye	20	29.8	432.1
Solar still with Black In	20	28.4	411.2

5. Conclusions

In this paper, the effect of different absorber materials on the performance of a solar still desalination system is studied with the help of COMSOL[®] Multiphysics 5.6 software. COMSOL[®] software is used for computational fluid dynamics (CFD) of solar still geometry based on the setup in reference [20]. The effect of absorber materials including black ink, black dye, and black toner on the performance of the solar still's hourly productivity, the exergy of evaporation, and the evaporative heat transfer coefficient are investigated through numerical analysis. The following conclusions are drawn from this paper:

- The rise in productivity of the solar still due to the use of absorber materials black ink, black dye, and black toner is validated by means of computational fluid dynamics using COMSOL[®] Multiphysics software.
- The highest energy and exergy production occurred in the solar still using black toner, which is about 785 kWh and 49.8 kWh, respectively. Note that this energy and exergy production is 26.9% and 27.0%, respectively, higher than that of a conventional solar still.
- The radiation model in COMSOL[®] Multiphysics software can be applied to a solar still geometry to analyze its performance throughout the day.
- The lowest CPL of the solar still was obtained using black toner, which was about 0.0066 USD/L.
- Effective emissivity applied to the solar still inner walls can be used as a controlling parameter to consider the absorptivity of the water mixture.

The simulation outcomes for variation in parameter effective emissivity are significantly less as compared to the results of reference data [12]. While the simulation results indicate in what manner the actual results could change.

- The CO₂ mitigation and enviroeconomic parameter of the solar still using black toner were equal to 31.4 tons and 455.3 USD, respectively.
- The use of black toner as an absorbing material in the solar still caused the highest improvement in productivity, with maximum value in [12] increased by 32.88% while that in the simulation increased by 10.52%. Similarly, maximum values of exergy of evaporation and heat transfer coefficient are increased in [12] by 41.48% and 32.65%, respectively, while that for the simulation shows augmentation by 13.68% and 5.37%, respectively.

Future work could include the use of nanotechnology for the preparation of a nanomaterial-based coating, which could be readily applied to the surface of the solar desalination system.

Author Contributions: Conceptualization (C.S., H.P. and M.M.J.); methodology (A.J.A., S.Z., H.P. and M.M.J.) formal analysis (H.P., S.Z., A.J.C. and A.D.O.) writing—original draft preparation (C.S., A.J.A. and M.M.J.), writing—review and editing, (D.D.B.-N., D.P.B.-N., A.D.O. and A.J.C.), Funding acquisition (D.P.B.-N. and D.D.B.-N.). All authors have read and agreed to the published version of the manuscript.

Funding: This work was also supported by Gheorghe Asachi Technical University of Iași—TUIASI-Romania, Scientific Research Funds, FCSU-2022.

Data Availability Statement: Not applicable.

Acknowledgments: This paper was financially supported by the Project “Network of excellence in applied research and innovation for doctoral and postdoctoral programs”/InoHubDoc, project co-funded by the European Social Fund financing agreement no. POCU/993/6/13/153437.

Conflicts of Interest: The authors declare that they have no conflict of interest.

Nomenclature

A_i	surface area of body i (m^2)
$C_{p,a}$	specific heat capacity at constant pressure of air ($J/(kg \cdot K)$)
$C_{p,v}$	specific heat capacity at constant pressure of vapor ($J/(kg \cdot K)$)
c_{sat}	vapor saturation concentration (mol/m^3)
c_v	vapor concentration (mol/m^3)
D	vapor diffusion coefficient in air (m^2/s)
Ex_{ew}	exergy of evaporation transferred from water to glass cover (W)
Ex_{gen}	exergy generation in system (W)
F_{ij}	view factor from surface i intercepted by surface j
G	moisture source or sink ($kg/(m^3 \cdot s)$)
g_w	vapor flux by diffusion ($kg/(m^2 \cdot s)$)
h_{cw}	convective heat transfer coefficient of water ($W/m^2 \cdot K$)
h_{ew}	evaporative heat transfer coefficient of water
J_i, J_j	total radiative flux leaving from surface i and surface j (W/m^2)
L	latent heat of vaporization of water (J/kg)
\dot{m}_{ew}	hourly distilled water yield of the solar still (kg/h)
M_v	molar mass of water vapor (kg/mol)
P	partial saturated vapor pressure (Pa)
p	pressure at interface between fluids (Pa)
q	heat flux by conduction (W/m^2)
q_r	heat flux by radiation (W/m^2)
q_{cw}	convective heat transfer of water (W)
q_{ew}	evaporative heat transfer from water (W)
Q_{ij}	power transmitted from body i to body j (W)
Q_i	thermal energy leaving surface i (W)
Q_H	diffusive flux of thermal enthalpy due to the rate of change of air and vapor in moist air ($J/(m^2 \cdot s)$)
Q	heat sources other than viscous dissipation (W/m^3)
t	time interval (s)
T	absolute temperature (K)
T_i	temperature of surface i (K)
T_j	temperature of surface j (K)
u	air velocity field (m/s)
ω_v	vapor mass fraction
Greek symbols	
α	Absorptivity
α_p	coefficient of thermal expansion ($1/K$)
ε	Emissivity
ε_{eff}	effective emissivity
ρ	fluid density (kg/m^3)
ρ_g	moist air density (kg/m^3)
σ	Stefan Boltzmann coefficient ($W/m^2/K^4$)
τ	viscous stress tensor (Pa)
τ_w	transmissivity of water
ϕ_w	relative humidity
Subscripts	
a	Air
b	basin liner
w	Water
v	Vapor

Appendix A

CFD analysis of the solar still model is performed using COMSOL[®] Multiphysics software. A user tutorial of COMSOL[®] had been studied to initiate analysis of the solar

still. The important conditions applied in COMSOL[®] Multiphysics for CFD analysis are explained below:

- The system variables have been evaluated using COMSOL[®] Multiphysics by means of analytic functions.
- ‘Ambient properties’ are defined through the ‘shared properties’ node of ‘Definitions’. Ambient condition is applied as per ASHRAE 2017 meteorological data that are provided in COMSOL[®].
- The geometric model is developed using solid blocks and right-angled prisms.
- All the materials used for simulation are taken from the material library. Surface emissivity for the inner black painted walls of the solar still is taken as 0.9.
- The physics nodes applied in COMSOL[®] Multiphysics software are explained below.
- The ‘surface-to-surface radiation’ is applied to the solar still model with consideration of wavelength dependent radiation properties. Two spectral bands have been considered that are separated at 2 μm of wavelength.
- ‘Fractional emissive power’ is defined under the ‘diffuse surface’ node for each spectral band. The sum of fractional emissive power for the two spectral bands is equal to unity.
- ‘Opacity’ node is applied to the glass cover considering the wavelength dependent opacity of the glass:
 - Transparent for visible light
 - Opaque for infrared radiation
- ‘External radiation source’ is applied with source position as ‘solar position’. Location of experimentation for simulation model is defined by latitude ‘23.5204’ and longitude ‘87.3119’.
- ‘Heat transfer in moist air’ is applied to the model with initial temperature according to the ambient data.
- ‘Convectively enhanced conductivity’ is applied to moist air and water so as to consider the convection effect in these fluids.
- ‘Heat flux’ is applied to all the outer surfaces. It considers external natural convection according to the orientation and length of walls.
- ‘Moisture transport in the air’ is applied to the air domain inside the solar still. The initial value of relative humidity is taken as 0.1. ‘Wet surface’ node is applied to the interface between water and air.
- Multiphysics ‘heat transfer with surface-to-surface radiation’ is applied to couple the physics ‘surface-to-surface radiation’ and ‘heat transfer in moist air’. In this multiphysics, default opacity is considered from the heat transfer interface.
- Multiphysics ‘heat and moisture’ are applied to couple the physics ‘heat transfer in moist air’ and ‘moisture transport in air’. Here, the latent heat source is considered for evaporation. It uses the heat of evaporation from water.

References

1. Panchal, H.N.; Thakkar, H. Theoretical and experimental validation of evacuated tubes directly coupled with solar still. *Therm. Eng.* **2016**, *63*, 825–831. [[CrossRef](#)]
2. Panchal, H.; Patel, N.; Thakkar, H. Various techniques for improvement in distillate output from active solar still: A review. *Int. J. Ambient Energy* **2017**, *38*, 209–222. [[CrossRef](#)]
3. Panchal, H.N.; Shah, P.K. Improvement of Solar Still Productivity by Energy Absorbing Plates. *J. Renew. Energy Environ.* **2014**, *1*, 1–7.
4. Panchal, H.N. Experimental Investigation of Varying Parameters Affecting on Double Slope Single Basin Solar Still. *Int. J. Adv. Eng. Sci.* **2011**, *2*, 17–21.
5. Al-Harashsheh, M.; Abu-Arabi, M.; Ahmad, M.; Mousa, H. Self-powered solar desalination using solar still enhanced by external solar collector and phase change material. *Appl. Therm. Eng.* **2022**, *206*, 118118. [[CrossRef](#)]
6. AbuShanab, W.S.; Elsheikh, A.H.; Ghandourah, E.I.; Moustafa, E.B.; Sharshir, S.W. Performance improvement of solar distiller using hang wick, reflectors and phase change materials enriched with nano-additives. *Case Stud. Therm. Eng.* **2022**, *31*, 101856. [[CrossRef](#)]
7. Abdel-Rehim, Z.S.; Lasheen, A. Experimental and theoretical study of a solar desalination system located in Cairo, Egypt. *Desalination* **2007**, *217*, 52–64. [[CrossRef](#)]

8. Elsheikh, A.H.; Panchal, H.; Ahmadein, M.; Mosleh, A.O.; Sadasivuni, K.K.; Alsaleh, N.A. Productivity forecasting of solar distiller integrated with evacuated tubes and external condenser using artificial intelligence model and moth-flame optimizer. *Case Stud. Therm. Eng.* **2021**, *28*, 101671. [[CrossRef](#)]
9. Pansal, K.; Ramani, B.; Sadasivuni, K.K.; Panchal, H.; Manokar, M.; Sathyamurthy, R.; Kabeel, A.; Suresh, M.; Israr, M. Use of solar photovoltaic with active solar still to improve distillate output: A review. *Groundw. Sustain. Dev.* **2020**, *10*, 100341. [[CrossRef](#)]
10. Elaziz, M.A.; Essa, F.; Elsheikh, A.H. Utilization of ensemble random vector functional link network for freshwater prediction of active solar stills with nanoparticles. *Sustain. Energy Technol. Assess.* **2021**, *47*, 101405. [[CrossRef](#)]
11. Sharshir, S.; Peng, G.; Wu, L.; Yang, N.; Essa, F.; Elsheikh, A.; Mohamed, S.I.; Kabeel, A. Enhancing the solar still performance using nanofluids and glass cover cooling: Experimental study. *Appl. Therm. Eng.* **2017**, *113*, 684–693. [[CrossRef](#)]
12. Sharshir, S.; Elsheikh, A.; Peng, G.; Yang, N.; El-Samadony, M.; Kabeel, A. Thermal performance and exergy analysis of solar stills—A review. *Renew. Sustain. Energy Rev.* **2017**, *73*, 521–544. [[CrossRef](#)]
13. Panchal, H.; Sadasivuni, K.K.; Suresh, M.; Yadav, S.; Brahmabhatt, S. Performance analysis of evacuated tubes coupled solar still with double basin solar still and solid fins. *Int. J. Ambient Energy* **2020**, *41*, 1031–1037. [[CrossRef](#)]
14. Panchal, H.; Nurdianto, H.; Sadasivuni, K.K.; Hishan, S.S.; Essa, F.; Khalid, M.; Dharaskar, S.; Shanmugan, S. Experimental investigation on the yield of solar still using manganese oxide nanoparticles coated absorber. *Case Stud. Therm. Eng.* **2021**, *25*, 100905. [[CrossRef](#)]
15. Kateshia, J.; Lakhera, V. A comparative study of various fatty acids as phase change material to enhance the freshwater productivity of solar still. *J. Energy Storage* **2022**, *48*, 103947. [[CrossRef](#)]
16. Bamasag, A.; Essa, F.A.; Omara, Z.; Bahgat, E.; Alsaiani, A.O.; Abulkhair, H.; Alsulami, R.A.; Elsheikh, A.H. Machine learning-based prediction and augmentation of dish solar distiller performance using an innovative convex stepped absorber and phase change material with nanoadditives. *Process Saf. Environ. Prot.* **2022**, *162*, 112–123. [[CrossRef](#)]
17. Sakthivel, M.; Shanmugasundaram, S.; Alwarsamy, T. An experimental study on a regenerative solar still with energy storage medium—Jute cloth. *Desalination* **2010**, *264*, 24–31. [[CrossRef](#)]
18. Sakthivel, M.; Shanmugasundaram, S. Effect of energy storage medium (black granite gravel) on the performance of a solar still. *Int. J. Energy Res.* **2008**, *32*, 68–82. [[CrossRef](#)]
19. Chandrashekar, M.; Yadav, A. Experimental study of exfoliated graphite solar thermal coating on a receiver with a Scheffler dish and latent heat storage for desalination. *Sol. Energy* **2017**, *151*, 129–145. [[CrossRef](#)]
20. Layek, A. Exergetic analysis of basin type solar still. *Eng. Sci. Technol. Int. J.* **2018**, *21*, 99–106. [[CrossRef](#)]
21. Sharshir, S.W.; Peng, G.; Elsheikh, A.; Edreis, E.M.; Eltawil, M.A.; Abdelhamid, T.; Kabeel, A.; Zang, J.; Yang, N. Energy and exergy analysis of solar stills with micro/nano particles: A comparative study. *Energy Convers. Manag.* **2018**, *177*, 363–375. [[CrossRef](#)]
22. Deniz, E. Energy and exergy analysis of flat plate solar collector-assisted active solar distillation system. *Desalination Water Treat.* **2016**, *57*, 24313–24321. [[CrossRef](#)]
23. Steiner, T.R. High temperature steady-state experiment for computational radiative heat transfer validation using COMSOL and ANSYS. *Results Eng.* **2022**, *13*, 100354. [[CrossRef](#)]
24. El-Said, E.M.; Elsheikh, A.H.; El-Tahan, H.R. Effect of curved segmental baffle on a shell and tube heat exchanger thermohydraulic performance: Numerical investigation. *Int. J. Therm. Sci.* **2021**, *165*, 106922. [[CrossRef](#)]
25. Essa, F.; Elsheikh, A.H.; Algazzar, A.A.; Sathyamurthy, R.; Ali, M.K.A.; Elaziz, M.A.; Salman, K. Eco-friendly coffee-based colloid for performance augmentation of solar stills. *Process Saf. Environ. Prot.* **2020**, *136*, 259–267. [[CrossRef](#)]
26. Abakr, Y.A.; Ismail, A.F. Theoretical and Experimental Investigation of a Novel Multistage Evacuated Solar Still. *J. Sol. Energy Eng.* **2005**, *127*, 381–385. [[CrossRef](#)]
27. Badusha, A.R.; Arjunan, T.V. Performance analysis of single slope solar still. *Int. J. Mech. Eng. Robot Res.* **2013**, *2*, 74–81.
28. Rahbar, N.; Esfahani, J. Productivity estimation of a single-slope solar still: Theoretical and numerical analysis. *Energy* **2013**, *49*, 289–297. [[CrossRef](#)]
29. Rahbar, N.; Esfahani, J.A.; Fotouhi-Bafghi, E. Estimation of convective heat transfer coefficient and water-productivity in a tubular solar still—CFD simulation and theoretical analysis. *Sol. Energy* **2015**, *113*, 313–323. [[CrossRef](#)]
30. Maheswari, C.U.; Reddy, V.; Sree, N.; Reddy, V.; Reddy, S.P.; Prasad, R.R.; Siva, A.; Raghu, C.; Harish, B.; Varma, K. CFD Analysis of Single Basin Double Slope Solar Still. *Invent. J. Res. Technol. Eng. Manag. (IJRTEM)* **2016**, *1*, 1–5.
31. Hafs, H.; Zaaoumi, A.; Ansari, O.; Bah, A.; Asbik, M.; Malha, M. Effect of the Nanofluid (Brackish water/ Al_2O_3) on the Passive Solar Still Desalination Performance with Heat Storage System. In Proceedings of the 2018 10th International Conference on Electronics, Computers and Artificial Intelligence (ECAI), Iasi, Romania, 28–30 June 2018; IEEE: Piscataway, NJ, USA; pp. 1–6.
32. Sharshir, S.W.; Peng, G.; Elsheikh, A.H.; Eltawil, M.A.; Elkadeem, M.; Dai, H.; Zang, J.; Yang, N. Influence of basin metals and novel wick-metal chips pad on the thermal performance of solar desalination process. *J. Clean. Prod.* **2019**, *248*, 119224. [[CrossRef](#)]
33. Shoeibi, S.; Rahbar, N.; Esfahani, A.A.; Kargarsharifabad, H. Energy matrices, exergoeconomic and enviroeconomic analysis of air-cooled and water-cooled solar still: Experimental investigation and numerical simulation. *Renew. Energy* **2021**, *171*, 227–244. [[CrossRef](#)]
34. Shoeibi, S.; Kargarsharifabad, H.; Rahbar, N.; Ahmadi, G.; Safaei, M.R. Performance evaluation of a solar still using hybrid nanofluid glass cooling—CFD simulation and environmental analysis. *Sustain. Energy Technol. Assess.* **2022**, *49*, 101728. [[CrossRef](#)]
35. Panchal, H.; Petkar, R.; Sonawane, C.; Sadasivuni, K.K.; Mohamad, H.A.E.D.; Boka, P. Use of computational fluid dynamics for solar desalination system: A review. *Int. J. Ambient Energy* **2021**, 1–16. [[CrossRef](#)]

36. Fan, S.; Wang, X.; Cao, S.; Wang, Y.; Zhang, Y.; Liu, B. A novel model to determine the relationship between dust concentration and energy conversion efficiency of photovoltaic (PV) panels. *Energy* **2022**, *252*, 123927. [[CrossRef](#)]
37. Fan, S.; Liang, W.; Wang, G.; Zhang, Y.; Cao, S. A novel water-free cleaning robot for dust removal from distributed photovoltaic (PV) in water-scarce areas. *Sol. Energy* **2022**, *241*, 553–563. [[CrossRef](#)]
38. Petkar, R.; Sonawane, C.R.; Panchal, H. Investigation of thermal Desalination system using heat recovery. In *Lecture Notes in Mechanical Engineering*; Springer: Singapore, 2019. [[CrossRef](#)]
39. Matheswaran, M.M.; Arjunan, T.V.; Muthusamy, S.; Natrayan, L.; Panchal, H.; Subramaniam, S.; Khedkar, N.K.; El-Shafay, A.; Sonawane, C. A case study on thermo-hydraulic performance of jet plate solar air heater using response surface methodology. *Case Stud. Therm. Eng.* **2022**, *34*, 101983. [[CrossRef](#)]
40. Sonawane, C.R.; Panchal, H.N.; Hoseinzadeh, S.; Ghasemi, M.H.; Alrubaie, A.J.; Sohani, A. Bibliometric Analysis of Solar Desalination Systems Powered by Solar Energy and CFD Modelled. *Energies* **2022**, *15*, 5279. [[CrossRef](#)]
41. Ullah, I.; Ullah, A.; Selim, M.M.; Khan, M.I.; Saima; Khan, A.A.; Malik, M.Y. Analytical investigation of magnetized 2D hybrid nanofluid (GO + ZnO + blood) flow through a perforated capillary. *Comput. Methods Biomech. Biomed. Eng.* **2022**, *online ahead of print*. [[CrossRef](#)]
42. Shah, Z.; Ullah, A.; Musa, A.; Vrinceanu, N.; Bou, S.F.; Iqbal, S.; Deebani, W. Entropy Optimization and Thermal Behavior of a Porous System with Considering Hybrid Nanofluid. *Front. Phys.* **2022**, *10*, 929463. [[CrossRef](#)]
43. Alharbi, K.A.M.; Ullah, A.; Ikramullah; Fatima, N.; Khan, R.; Sohail, M.; Khan, S.; Khan, W.; Ali, F. Impact of viscous dissipation and coriolis effects in heat and mass transfer analysis of the 3D non-Newtonian fluid flow. *Case Stud. Therm. Eng.* **2022**, *37*, 102289. [[CrossRef](#)]
44. Rizk, D.; Ullah, A.; Ikramullah; Elattar, S.; Alharbi, K.A.M.; Sohail, M.; Khan, R.; Khan, A.; Mlaiki, N. Impact of the KKL Correlation Model on the Activation of Thermal Energy for the Hybrid Nanofluid (GO+ZnO+Water) Flow through Permeable Vertically Rotating Surface. *Energies* **2022**, *15*, 2872. [[CrossRef](#)]
45. Ullah, A.; Ikramullah; Selim, M.M.; Abdeljawad, T.; Ayaz, M.; Mlaiki, N.; Ghafoor, A. A Magnetite-Water-Based Nanofluid Three-Dimensional Thin Film Flow on an Inclined Rotating Surface with Non-Linear Thermal Radiations and Couple Stress Effects. *Energies* **2021**, *14*, 5531. [[CrossRef](#)]
46. Hussain, Z.; Khan, S.; Ullah, A.; Ikramullah; Ayaz, M.; Ahmad, I.; Mashwani, W.K.; Chu, Y.-M. Extension of optimal homotopy asymptotic method with use of Daftardar–Jefferly polynomials to Hirota–Satsuma coupled system of Korteweg–de Vries equations. *Open Phys.* **2020**, *18*, 916–924. [[CrossRef](#)]
47. Khan, S.; Selim, M.M.; Gepreel, K.A.; Ullah, A.; Ikramullah; Ayaz, M.; Mashwani, W.K.; Khan, E. An analytical investigation of the mixed convective Casson fluid flow past a yawed cylinder with heat transfer analysis. *Open Phys.* **2021**, *19*, 341–351. [[CrossRef](#)]
48. Greenhouse Effect. Available online: <https://www.comsol.jp/model/greenhouse-effect-98061> (accessed on 18 August 2022).
49. van Eck, R.; Klep, M.; van Schijndel, J. Surface to surface radiation benchmarks. In Proceedings of the 2016 COMSOL Conference, Munich, Germany, 12–14 October 2016; pp. 4–12.
50. Kumar, S.; Dubey, A.; Tiwari, G.N. A solar still augmented with an evacuated tube collector in forced mode. *Desalination* **2014**, *347*, 15–24. [[CrossRef](#)]
51. Fath, H.E.S.; El-Samanoudy, M.; Fahmy, K.; Hassabou, A. Thermal-economic analysis and comparison between pyramid-shaped and single-slope solar still configurations. *Desalination* **2003**, *159*, 69–79. [[CrossRef](#)]